Journal of Sustainable Mining 17 (2018) 226–238

HOSTED BY

Contents lists available at ScienceDirect

Journal of Sustainable Mining

journal homepage: www.elsevier.com/locate/jsm

Research paper

Analysis of the average fire gas temperature in a mine drift with multiple fires

Rickard Hansen

Sustainable Minerals Institute, The University of Queensland, Brisbane, QLD, 4072, Australia

ARTICLE INFO

Keywords:
Multiple fires
Mine drift
Average fire gas temperature

ABSTRACT

The average fire gas temperature of multiple fires in a mine drift with longitudinal ventilation is investigated. The output of a quasi-steady model is investigated and compared with experimental results from model scale fire experiments. During the analysis it was found that the calculated average fire gas temperature of the model correlates quite well with the measured temperature, except for the period when the fire closest to the measuring point reached a peak of heat release rate. This poor correlation is likely due to flame impingement as the distance to the nearest fire decreases. Uncertainty of the calculations is caused by the fire gas temperature at the site of each individual fire and further studies into the fire growth rate and maximum heat release rates of multiple fires are recommended in order to remedy this uncertainty. When calculating the average fire gas temperature, a key parameter is determined with respect to the smoke spread in a mine drift as well as the risk of fire spread.

1. Introduction

The resulting smoke spread from a fire in an underground mine poses a great risk to miners underground, who face the risk of being trapped and inhaling toxic smoke. Depending on the layout of the mine, ventilation flows, lack of smoke barriers etc., the smoke spread could in a worst-case scenario affect large parts of the mine. A fire involving several individual fires could in many cases imply a high intensity fire with extensive smoke production. The smoke spread and behaviour of the smoke will largely be dictated by the temperature of the fire gases being emitted from the fire. The temperature of the fire gases will largely determine the likelihood that a fuel package at a certain distance from the fire will ignite, initiating a second fire. Flowing through mine drifts, ramps etc. the fire gases will undergo heat loss, where the magnitude of the heat losses will depend upon parameters such as longitudinal ventilation velocity, cross/sectional dimensions of the mine drift, roughness of the rock surface, distance from the fire, etc.

This study was undertaken to investigate the average temperature of the fire gases emitted from multiple fires in a mine drift with longitudinal ventilation. The following questions were also tackled: Is it possible to predict the average fire gas temperature at a certain distance from fires? What parameters should be focused on when determining average fire gas temperature? What unique characteristics will this type of scenario present?

Knowledge of the average fire gas temperature at certain distances from a set of multiple fires will enable the determination of smoke spread and smoke behaviour, which in turn could be used when addressing fire safety in an underground mine. When investigating average fire gas temperature, experimental data from earlier performed model-scale fire experiments by Hansen and Ingason (2012) were applied as these experiments were found to fit very well with the aim of this study. The purpose of this study is to investigate the possibility of predicting the average fire gas temperature for a number of individual fires along a mine drift and to investigate the characteristics of this type of fire scenario with respect to the average fire gas temperature. This knowledge would increase the understanding of the behaviour of multiple fires in underground mines, which is needed as earlier studies have focused on a single fire source or fires in tunnels.

Earlier studies on predicting fire gas temperatures in underground mines have encompassed models containing considerable simplifications and where the predictions were seldom validated against experiments. Chang and Greuer (1985) set up an initial boundary condition where the enthalpy change due to evaporation as well as the convective heat transfer from the mine air to the wall were accounted for. The study was aimed at mine air in general and not a fire scenario in particular, which explains why the radiative heat transfer from the gas volume to the wall was not accounted for; no validation work was presented in the study. Simode (1985) presented a model to determine the smoke temperatures along mine drifts, where only the convective heat transfer mechanism was included in the heat transfer calculations. The model was validated against an earlier performed experiment as well as an earlier fire which occurred underground. McPherson (1986)

E-mail address: rickard.hansen@uq.edu.au.

https://doi.org/10.1016/j.jsm.2018.08.001
Received 29 April 2018; Received in revised form 24 June 2018; Accepted 8 August 2018
Available online 09 August 2018

Nomenclature

A	area (m^2)
a	side length of mine drift cross section (m)
b	side length of mine drift cross section (m)
C	correction factor
c_p	specific heat capacity of the fluid at constant pressure (J/kg K)
D	diameter of tunnel or mine drift (m)
D_h	hydraulic diameter of the tunnel or mine drift (m)
E	emissive power (kW/m^2)
f	Darcy friction factor
F	view factor
h_{total}	total heat transfer coefficient (W/m^2 K)
h_c	convective heat transfer coefficient (kW/m^2 K)
h_r	radiative heat transfer coefficient (kW/m^2 K)
k	thermal conductivity (kW/m K)
k_g	thermal conductivity of fire gases (kW/m K)
k_w	thermal conductivity of wall (kW/m K)
$\dot{m}_a$	mass flow in tunnel or mine drift (kg/s)
$\dot{m}_{mix}$	mass flow of fire gases (kg/s)
Nu	Nusselt number
P	perimeter of tunnel or mine drift (m)
Pr	Prandtl number
$\dot{Q}$	heat release rate (kW)
$\dot{Q}_{conv}$	convective heat release rate (kW)
$\dot{q}''_{incident}$	incident heat flux (kW/m^2)
$\dot{q}''_{rad}$	radiative heat flux (kW/m^2)
Re	Reynolds number
t	time (s)
T_{avg}	average fire gas temperature over the entire cross-section at a given position (K)
$T_{avg,x=0}$	average fire gas temperature at the site of the fire (K)
T_g	fire gas temperature (K)
T_m^i	node temperature at time step i (K)
T_0	ambient temperature (K)
T_w	wall temperature (K)
T_∞	free-stream temperature (K)
u	fluid velocity (m/s)
v	average fluid velocity (m/s)
x	distance along the mine drift (m)
α	absorptivity factor
δ	boundary layer thickness (m)
ε	emissivity factor
ρ	fluid density (kg/m^3)
σ	Stefan-Boltzmann constant, $5.67{\cdot}10^{-11}$ kW/m^2 K^4
$\tau_{transport}$	transport time (s)

Subscripts

Fg	fire gases
Fl	flame
Rs	rock surface

presented a model where the radiative heat transfer mechanism was not included. The study was mainly aimed at heat flow in general in an underground airway and not specifically for a fire scenario. No validation of the proposed model was presented in the study. Chang and Greuer (1987) presented a model of the heat transfer in a mine airway during a fire, applying the energy conservation law. The heat transfer between the wall and the smoke was assumed to be composed of a convective as well as a radiative heat transfer component; no validation of the model was included in the paper. Dziurzynski, Tracz, and Trutwin (1988) presented a mine fire model and conducted simulations with the model. In the model the fire was assumed to have a lumped character and only the convective heat transfer between the air and the rock was accounted for; no validation of the model was presented in the report. Wolski (1995) presented a simplified model on the heat exchange between flowing air and tunnel walls. The model applies a constant and a lumped heat transfer coefficient. The model was validated against model scale experiments and found to be in line with these experiments. Beard and Carvel (2005) proposed the following set of expressions for the average fire gas temperature at a given position along a tunnel with longitudinal ventilation:

$$T_{avg}(x,\, t) = T_0 + [T_{avg,x=0}(\tau) - T_0]\, e^{-\frac{h_{total}\, P\, x}{\dot{m}_a\, c_p}} \tag{1}$$

$$\tau_{transport} = t - \left(\frac{x}{u}\right) \tag{2}$$

$$T_{avg,x=0}(\tau_{transport}) = T_0 + \frac{2}{3}\,\frac{\dot{Q}(\tau)}{\dot{m}_a\, c_p} \tag{3}$$

The following assumptions were made:

- Longitudinal ventilation velocity is non-variant along the tunnel.
- A lumped heat transfer coefficient.
- A wall temperature equal to the ambient temperature.

Hansen (2017a) conducted a study on the influence of rock surface roughness on fire gases' temperature in a mine drift. A number of correlations were investigated and validated against experimental results from full-scale fire experiments. The calculations included the convective heat transfer mechanism as well as the radiative component.

Earlier studies on multiple fires in mines and tunnels have mainly focused on tunnel fires and on the phenomenon of merging flames from multiple fires. Wan et al. (2017) performed a number of multi-fire experiments in a model scale tunnel, presenting a model for predicting the ceiling gas temperature profile. Ji et al. (2016) conducted experiments with two pool fires in a model scale tunnel, studying the interaction between the individual fires. Hansen and Ingason (2011, 2012) studied the ignition of individual fuel items and the calculation of the heat release rate of multiple objects located in an underground structure. The results of the calculations were validated against model scale tunnel/mine drift fire experiments. Hansen (2017b) studied phenomena – including fire gas temperatures – occurring during continuous fire spread between multiple fires in a model scale mine drift.

In the following chapter, the heat losses of the fire gases in a mine drift are outlined and the influencing parameters are discussed. A model for calculating the heat losses of the fire gases in a mine drift is set up and the model scale experiments by Hansen and Ingason (2012) are described. The resulting average fire gas temperatures of the model are validated against results from small scale fire experiments.

2. The heat losses of fire gases in a mine drift with longitudinal ventilation

When flowing through the mine drift, fire gases will, with increasing distance from the fire site, undergo heat losses, but will also – to a lesser extent – re-gain some heat.

Having a higher temperature than the surrounding rock surface, the fire gases will lose heat to the rock surface through convective and

radiative cooling. As well as the fire gases, the flames of the fire will also heat the rock surface closest to the fire. The heated rock surface will eventually – with increasing surface temperature – decrease the convective heat losses of the fire gases and re-radiate heat to the fire gases. The decrease in convective heat losses and the re-radiation of the fire gases will mainly take place in the region closest to the fire, further downstream the cooling effect of the surrounding rock surface will dominate.

Besides the distance from the fire site, a number of other characteristics of the mine drift will have an influence on the fire gas temperature. An increase in the cross-sectional dimensions will decrease the fire gas temperature as the surface area of the cooling rock surface increases. The increasing surface roughness of the rock surface will increase the rock surface area and the turbulence of the fire gases which in turn will increase the heat losses from the fire gases to the surrounding rock surfaces. Different types of rock material will have different densities and thermal capacities and therefore they will heat up differently and influence the fire gases differently as well.

An increase in longitudinal ventilation velocity will lead to an increase in the amount of cold air being mixed with the hot fire gases, thus increasing the cooling of the fire gases. However, an increase in longitudinal ventilation velocity will on the other hand also lead to hot fire gases being pushed further downstream while being mixed with cold air.

The exponentially decaying function in equation (1) contains a number of the above listed parameters: the distance from the fire site, the radiative and convective cooling are included in the lumped heat transfer coefficient, the cross sectional dimensions of the mine drift is included in the perimeter parameter and the longitudinal ventilation velocity is included in the mass flow parameter.

2.1. Boundary condition, solid surface/fire gas interface

Directly downstream of the fire the smoke spread will be marked by stratification and a flow that will not be fully developed. In this region the boundary layer will have a clear influence on the heat transfer between the fire gases and the solid surface. Further downstream the temperature gradient perpendicular to the flow direction will be near zero except for the region closest to the solid surface.

Below, the governing equations for the solid/gas interface for a solid surface exposed to radiant and convective heating are presented. The y-axis is perpendicular and the x-axis is parallel to the solid surface in the analysis.

Wall temperature at the solid surface, $t > 0$:

$$T(0, t) = T_w \tag{4}$$

Boundary conditions at the boundary layer edge ($y = \delta$), $t > 0$:

$$T(\delta, t) = T_\infty \tag{5}$$

$$\frac{\partial T}{\partial y}|_{y=\delta} = 0 \tag{6}$$

Assuming:

- Incompressible, steady flow.
- The temperature change in the x-direction of the solid to be small and thus the conduction in the flow direction negligible.

Accounting for the heat radiation, and neglecting the viscous work and second-order differentials; the energy balance for an element inside the boundary layer can be expressed as:

$$\rho\, c_p \left(u\frac{\partial T}{\partial x} + v\frac{\partial T}{\partial y}\right)\mathrm{d}x\mathrm{d}y = k\frac{\partial^2 T}{\partial y^2}\mathrm{d}x\mathrm{d}y + \dot{q}''_{\mathrm{rad}} \tag{7}$$

The solid boundary condition at a plane on the solid surface is ($y = 0$):

$$-k\mathrm{d}x\frac{\partial T}{\partial y}|_{y=0} = \rho\, c_p\,(v\ T)\mathrm{d}x + \rho\, c_p \left(u\frac{\partial T}{\partial x}\mathrm{d}x + T\frac{\partial u}{\partial x}\mathrm{d}x\right)dy + \dot{q}''_{\mathrm{rad}}|_{y=0} \tag{8}$$

where:

$$\dot{q}''_{\mathrm{rad}}|_{y=0} = \alpha\dot{q}''_{\mathrm{incident}} - \varepsilon\sigma(T_w^4 - T_g^4) \tag{9}$$

assuming radiant grey bodies.

The temperature gradient at the interface – $\frac{\partial T}{\partial y}|_{y=\delta}$ – will decrease as the thermal boundary layer thickness increases and thus also with increasing horizontal distance.

The temperature continuity at the interface is expressed by the following equation:

$$T_g|_{y=0} = T_w|_{y=0} \tag{10}$$

Similarly for the heat flux continuity (no-slip condition):

$$k_w\frac{\partial T_w}{\partial y}|_{y=0} = k_g\frac{\partial T_g}{\partial y}|_{y=0} + \dot{q}''_{\mathrm{rad}}|_{y=0} \tag{11}$$

3. Model scale experiments

A number of small scale fire experiments were conducted by Hansen and Ingason (2012), where a 1:15 model scale tunnel/mine drift (the size of the tunnel was 10 m long, 0.6 m wide and 0.4 m in height). During the experiments the distance between piles of wooden pallets was varied. The piles of wooden pallets consisted of scaled down softwood pallets (pine). See Fig. 1 and Fig. 2 for the set up of the experiments.

Three experiments were used as reference tests and these consisted of a single pile of pallets, whereas in the other tests four piles of wood pallets were placed at different distances from each other. The longitudinal ventilation velocity was varied for the three reference tests:

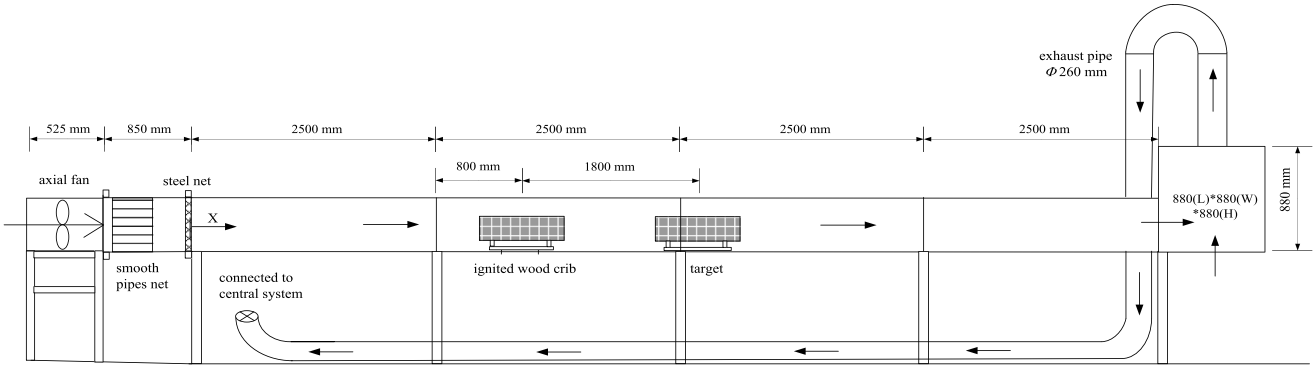

Fig. 1. A schematic drawing of the model tunnel (Ingason, 2005).

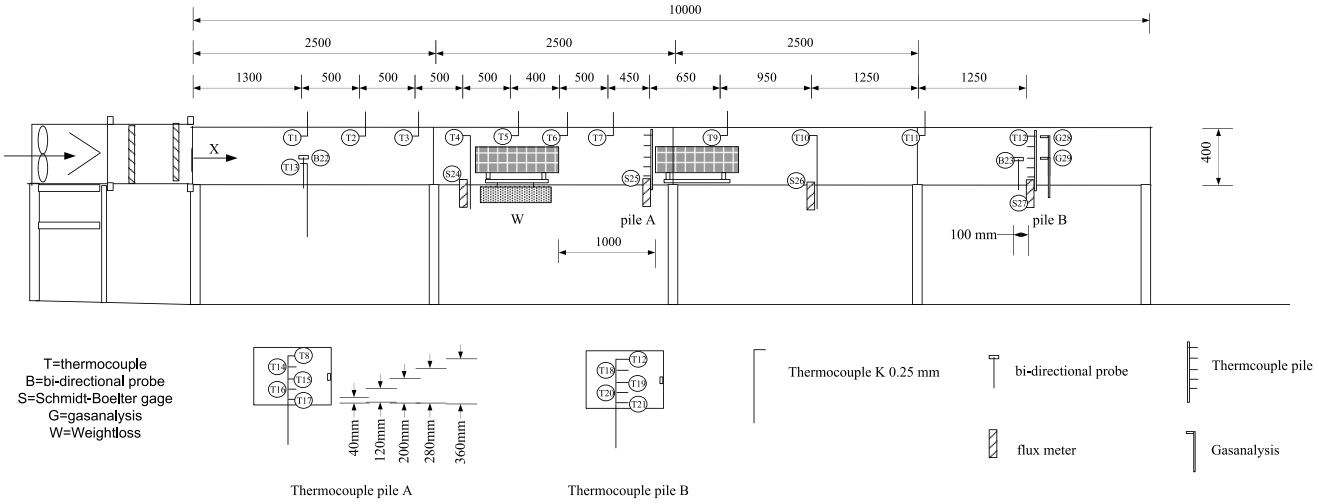

Fig. 2. Position of thermocouples, probes and instruments (Ingason, 2005).

0.3 m/s (experiment #1), 0.6 m/s (experiment #4) and 0.9 m/s (experiment #12).

A number of parameters were measured or calculated during the experiments, such as the time of ignition of the adjacent piles, the total heat release rate and the fire gas temperatures. For the average fire gas temperature measurements, two sets of thermocouples were positioned 4.65 m (named pile A in Figs. 2) and 8.75 m (named pile B in Fig. 2) from the inlet opening where the temperatures at various vertical positions were measured.

Table 1 shows the results from the model scale experiments. Test #2 is not included in the table and the study as the fire of the first pile failed to ignite the adjacent pile of pallets due to there being too great free distance and low longitudinal ventilation velocity. It can be observed that the ignition times of the second, third and fourth pile are all clocked starting from the ignition of the first pile, thus in test #3 the second pile ignited 96 s after the ignition of the first pile; the third pile ignited 129 s after the ignition of the first pile etc.

For a more detailed description of the wooden pallets and the experimental procedures see Hansen and Ingason (2010).

4. Method

A model was created in order to calculate the average fire gas temperature at pile B (see Fig. 2) for the various model scale fire experiments seen in Table 1. The average fire gas temperature at pile A was not investigated, as pile A was situated in between the piles of pallets and the average fire gas temperature measurements were affected by phenomena such as flame impingement. A quasi-steady process was applied in the model as the experiments included a transient heat release rate and longitudinal ventilation velocity and most equations for the calculation of the surface temperature assume constant heat flux. The quasi-steady process involves using a numerical method when at any instance in time the surface temperature can be described as though the surface was being exposed to a steady state situation. The quasi-steady process also allows for the variation of heat transfer coefficients, fire gas emissivity, etc. along the model scale mine drift.

Microsoft Office Excel spreadsheet software was used during the calculation of the numerical model.

When modelling a multiple fire scenario, the fires downstream of the initial fire were initiated according to their time of ignition. The average fire gas temperature at the fire sites further downstream was calculated using equation (3), applying the measured heat release rate of reference experiment #4 and where the ambient temperature was set to the average fire gas temperature of the fires upstream.

In the model the resulting second-order differentials of the convective energy were neglected in equation (8) and through simplifying

Table 1
Results from the model scale fire experiments. The ignition time of the first pile of wooden pallets was set to 0 s.

Test#	u [m/s]	Number of piles	Free distance between the piles [m]	Maximum heat release rate [kW]	Ignition times of second, third and fourth pile [s]
1	0.3	1	–	116	–
3	0.6	4	0.4; 0.7; 0.6.	504	96; 129; 150
4	0.6	1	–	154	–
5	0.6	4	0.5; 0.7; 0.8.	467	111; 164; 183
6	0.6	4	0.5; 0.8; 0.9.	488	105; 149; 176
7	0.6	4	0.5; 0.8; 1.1.	485	96; 139; 180
8	0.6	4	0.5; 0.8; 1.3.	479	99; 140; 195
9	0.6	4	0.6; 0.8; 1.1.	461	110; 162; 190
10	0.6	4	0.7; 0.8; 1.1.	454	130; 183; 224
11	0.6	4	0.7; 0.9; 1.1.	464	134; 196; 235
12	0.9	1	–	169	–

the gas phase details, by applying a convective heat transfer coefficient, equation (8) becomes:

$$-k\frac{\partial T}{\partial y}|_{y=0} = h_c\,(T_g - T_w) + \dot{q}''_{\text{rad}}|_{y=0} \tag{12}$$

The radiative heat flux term in equation (12) describes the net radiative interchange for the solid surface. The term will contain a number of different radiative heat transfer mechanisms: incident heat flux from the flames, incident heat flux from the fire gases and re-radiation from the solid surface to the surroundings. Evolving the term further:

$$\dot{q}''_{\text{rad}}|_{y=0} = \alpha_{Rs} E_{Fg} F_{Fg-Rs}\,\varepsilon_{Fg} + \alpha_{Rs}\,E_{Fl}\,F_{Fl-Rs}\,\tau_{Fg\,\text{Layer}}\,\varepsilon_{Fl} - \varepsilon_{Rs}\,E_{Rs}\,F_{Rs-Fg} \tag{13}$$

The absorptivity of the surface – α_{Rs} – was set to unity in the ensuing calculations.

The emissive power of the fire gases – E_{Fg} – is expressed by:

$$E_{Fg} = \sigma\,T_g^4 \tag{14}$$

The view factor of the fire gases to the solid surface and vice versa – F_{Fg-Rs}– could be assumed to be unity as the solid surface will be in direct contact and engulfed by the fire gases.

The re-radiation term in equation (13) was very early found to have very little influence on the model output and was therefore omitted in the calculations.

The solid boundary condition at a plane on the solid surface (equation (12)) can be approximated by the following finite-difference approximation for a surface node:

$$T_{m,n}^{i+1} = T_{m,n}^{i} + \frac{2\,(h_c + h_r)\,\Delta t}{\Delta x \rho c_p}\,(T_g^i - T_{m,n}^i) \tag{15}$$

The energy balance of a control volume of fire gases – where the boundary is the surface segment – was expressed by:

$$h_c\,(T_g - T_w)\,dA + \dot{q}''_{\text{rad}}|_{y=0}\,dA = \dot{m}_a\,c_p\,dT_g \tag{16}$$

Temperature difference – dT_g– was used when calculating the average gas temperature of the adjacent segment and time step. The radiative component in equation (12) will only contain the incident heat flux from the fire gases. The incident heat flux from the flames was accounted for when calculating the new temperature of the solid surface.

As opposed to parameters such as density, thermal conductivity etc., the specific heat and the Prandtl number vary very little with the temperature and were therefore kept constant throughout the calculations.

The assumptions listed above and the following were also applied in the model:

- In the stratification region, no conduction between the upper fire gas layer and the lower layer takes place.
- The model mine drift is surrounded by inert Promatect H boards on all sides except one side where fire resistant window glaze could be found.
- The initial temperature distribution in the model construction is taken to be equivalent to the ambient temperature of the model mine drift.
- The axial heat transfer is assumed to be negligent compared with the radial heat transfer.

For each time step and model segment a number of parameters were calculated:

- Convective heat transfer coefficient.
- Emissivity of the fire gases.
- Flame radiation to the surrounding construction.

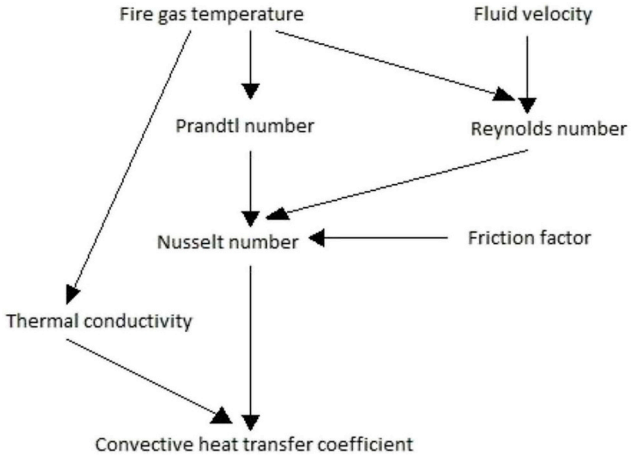

Fig. 3. The calculation of the convective heat transfer coefficient.

- Energy balance of control volume and fire gas temperature.
- Surface temperature.

Figs. 3 and 4 display the calculation flow when calculating the convective heat transfer coefficient (except when using the expression by Newman and Tewarson (1983)) and increment in fire gas temperature for each model segment and time step.

5. Results and discussion

The average fire gas temperature curves of the various experiments were calculated and depicted together with the average fire gas temperature of the corresponding experiments. The work was initially focused on the three reference tests, in order to investigate the performance of the model, what input parameters to focus on and to fine tune. The work then proceeded with experiments involving multiple piles of wooden pallets.

5.1. Size of segments

A segment width of 0.3 m was initially applied for reference test #1 in order to fit a time increment of 1 s and a longitudinal ventilation velocity of 0.3 m/s. As can be seen in Fig. 5, a segment width of 0.3 m fails to capture the average fire gas temperature at the peak period. Instead, the calculated average fire gas temperature displays an unexpected dip during the measured maximum temperature. Studying the calculations, a segment which is too large will overestimate the heat losses at the segments closest to the fire site. Thus the size of the segment was decreased to 0.15 m (and the time increment to 0.5 s for experiment #1) instead and the resulting average fire gas temperature can be seen in Fig. 6. When calculating the average fire gas temperatures of the multiple fire cases, the segment width had to be decreased to 0.075 m (and the time increment to 0.125 s due to a longitudinal ventilation velocity of 0.6 m/s) in order to capture the temperature variations during the peak period, as the calculated fire gas temperatures and heat losses were much higher than for the reference tests. The findings stress the importance of performing sensitivity analysis when applying the model.

5.2. Surface temperature

During the calculations it was found that the surface temperature varied greatly along the model scale mine drift, with considerable temperature increases at the sites of the individual fires. A multiple fire scenario will have distinctive variations in the surface temperature and must therefore be taken into account in the calculations. Large

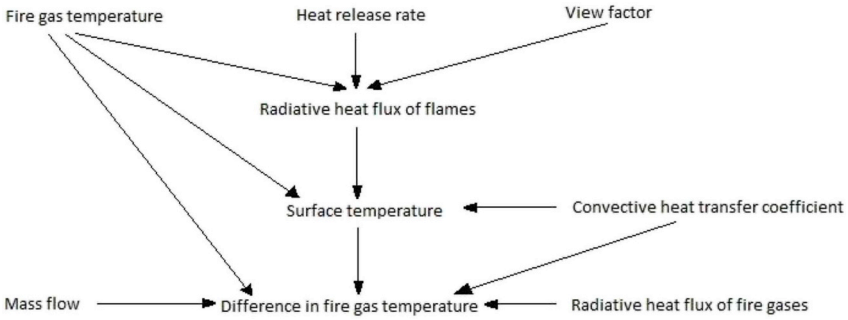

Fig. 4. The calculation of the increase in the fire gas temperature.

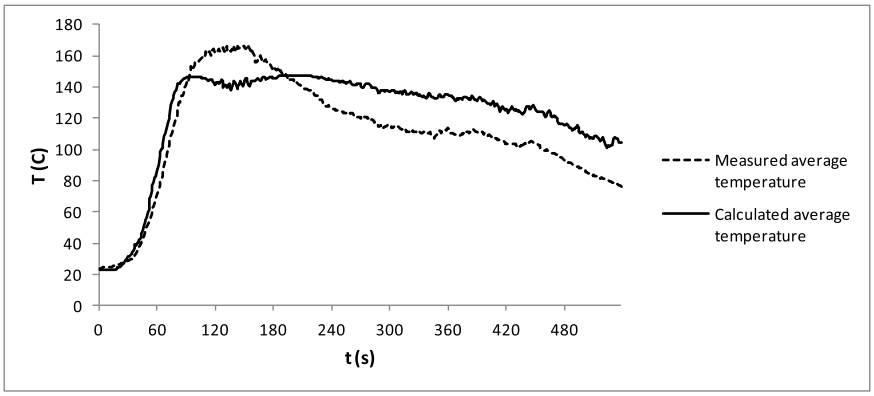

Fig. 5. The average fire gas temperature at pile B for experiment #1, applying a segment width of 0.3 m. The measured average temperature was taken from the experiments of Hansen and Ingason (2010).

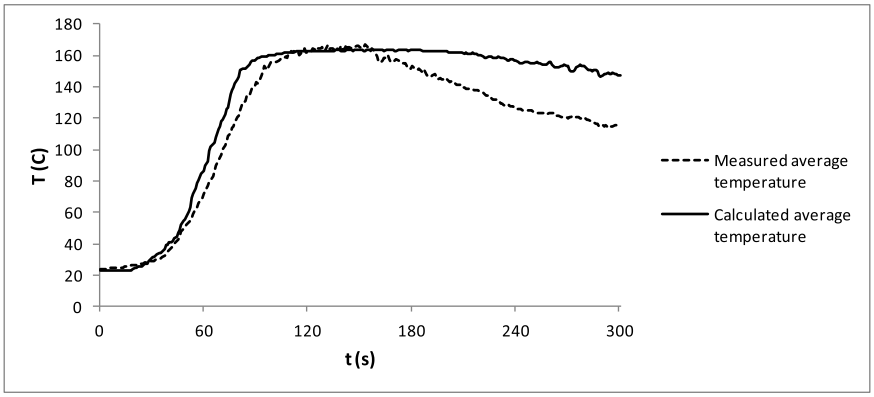

Fig. 6. The average fire gas temperature at pile B for experiment #1, applying a segment width of 0.15 m. The measured average temperature was taken from the experiments of Hansen and Ingason (2010).

variations in the surface temperature will have an effect on the radiative and convective heat losses of the fire gases. Fig. 7 displays the calculated surface temperature of experiment #3 at $t = 300$ s.

5.3. Convective heat transfer coefficient

Given the forced flow conditions and the extensive length of a mine drift, the transition to turbulent flow will take place close to the leading edge and will apply to the majority of the mine drift. Due to the enclosed nature, geometrical appearance and extensive length, the duct flow case is the most appropriate for the model scale mine drift.

Turbulent duct flow for circular ducts has been extensively explored, however, this is not the case for rectangular ducts. The results for circular ducts can be applied for rectangular ducts and they will provide fairly accurate results, through the application of hydraulic diameter (Bhatti & Shah, 1987) as the characteristic length:

$$D_h = \frac{2\,a\,b}{a + b} \tag{17}$$

Due to the enclosed nature of a mine drift, the boundary layer will fill up the mine drift and the flow will become fully developed, as the distances increases in the x-direction. The flow of fire gases in longer mine drifts will be fully developed for a considerable distance due to the geometrical appearance of the mine drift (i.e. the length of the mine drift is much larger than the diameter of the drift). The condition for a fully developed turbulent flow is as follows:

$$(\frac{x}{D}) \geq 10 \tag{18}$$

In the fully developed region the mean temperature of the hot fluid decreases in the x-direction, the vertical temperature gradient becomes more or less constant, and the convective heat transfer coefficient will become independent of the position in the x-direction.

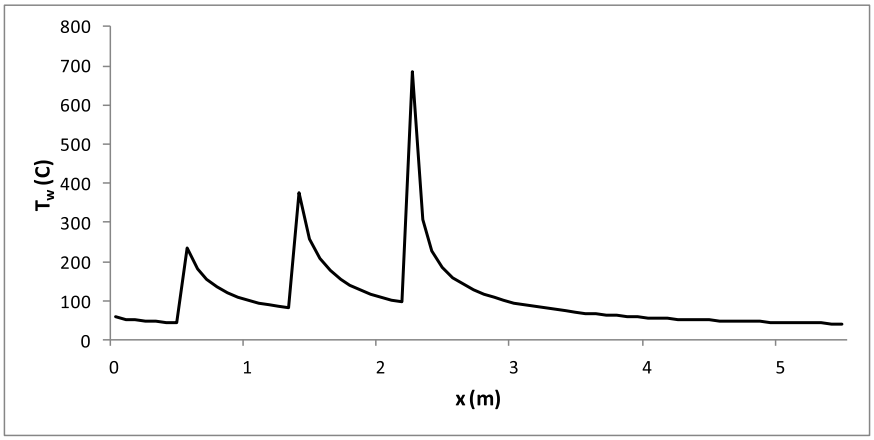

Fig. 7. The surface temperature along the model scale mine drift at $t = 300$ s, experiment #3.

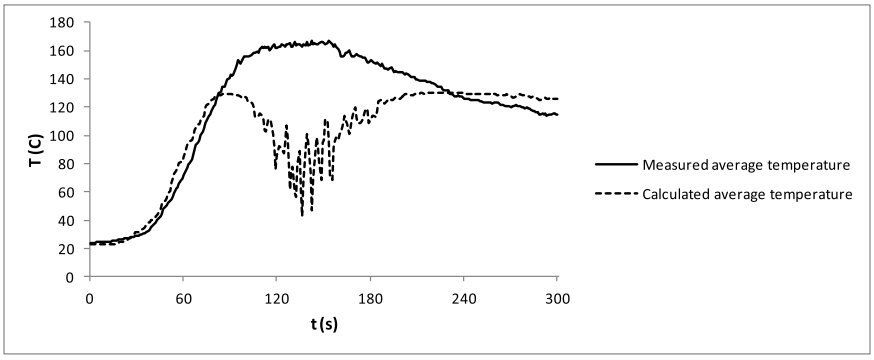

Fig. 8. The calculated average fire gas temperature of experiment #1, using a constant fire gas emissivity value of 0.3. The measured average temperature was taken from the experiments of Hansen and Ingason (2010).

In the entry section of a duct or in a section with stratification, the vertical temperature gradient will not be constant, and the convective heat transfer coefficient will not be independent of the position in the direction of the flow. In this section the Nusselt number will be larger than for a fully developed case. In the case of a mine drift it could be assumed, in most cases, that the thermal conditions will develop if a fully developed velocity profile is present, as the position of, for example, the fan will be further upstream of the fire. This case is classified as having a thermal entry region (Incropera, Dewitt, Bergman, & Lavine, 2007) and the average Nusselt number for the entry region may be calculated by applying the following correlation (Mills, 1962):

$$\frac{\overline{Nu}_{D_h,\text{entry}}}{Nu_{D_h}} = 1 + \frac{0.9756}{(\frac{x}{D_h})^{0.760}} \tag{19}$$

Applying the Nusselt number expression when calculating the convective heat transfer coefficient:

$$Nu_{D_h} = \frac{h_c\, D_h}{k} \tag{20}$$

The expression for the Nusselt number, valid for a fully developed turbulent duct flow:

$$Nu = \frac{(\frac{f}{2})\,(Re - 1000)\,Pr}{1 + 12.7\sqrt{(\frac{f}{2})}\,(Pr^{2/3} - 1)} \tag{21}$$

The friction factor in the correlation above was obtained from a Moody diagram.

Newman and Tewarson (1983) presented the following equation for calculating the average convective heat transfer coefficient to the walls along a rectangular duct:

$$h_c = 0.026\, Re_{D_h}^{-0.2}\,(1 + (\frac{D_h}{x})^{0.7})\,\rho\, c_p\, v \tag{22}$$

When performing the calculations it was found that applying equations (19)–(21) resulted in almost identical results when compared to the correlation used by Newman and Tewarson.

5.4. Radiative heat transfer

Setting the fire gas emissivity to a constant value throughout the entire experiment was found to have a large and undesired impact on the average fire gas temperature during periods with higher temperatures. The emissivity of the fire gases will decrease for higher fire gas temperatures, resulting in an increase in the average fire gas temperature. Fig. 8 displays the average fire gas temperature of experiment #1 when the fire gas emissivity was set to a constant value of 0.3.

The emissivity of the fire gases will depend on the composition of the gases, wavelength, partial pressure and temperature. Simplifying by applying the gray gas assumption, the fire gas emissivity is calculated using:

$$\varepsilon_{Fg} = C_{CO_2}\,\varepsilon_{CO_2} + C_{H_2O}\,\varepsilon_{H_2O} - \Delta\varepsilon_{CO_2-H_2O} \tag{23}$$

The correction factors were set to unity in the ensuing calculations and the emissivity factors were extracted from Hottel charts (Hottel, 1954). After accounting for the varying fire gas emissivity, the resulting average fire gas temperatures came very close to the measured values.

It was found that the radiative heat transfer coefficient varied greatly along the model scale mine drift during the experiments and the convective heat transfer coefficient did also vary along the mine drift during the experiments. Fig. 9 displays the variation of the radiative heat transfer coefficient along the model scale mine drift at $t = 300$ s for

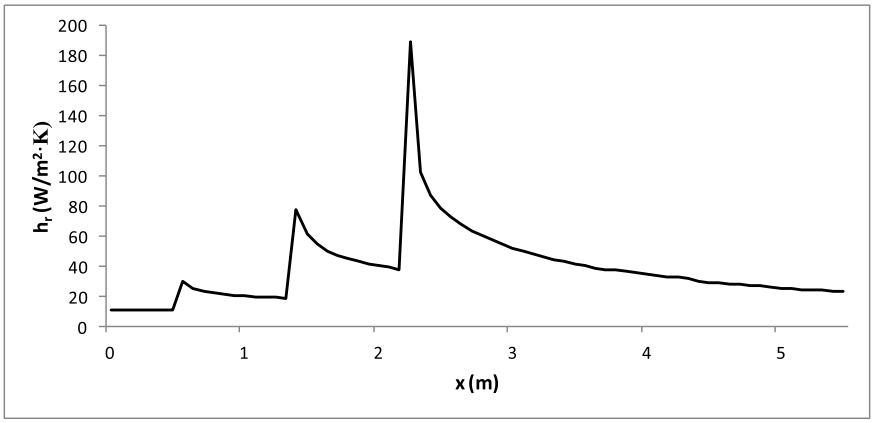

Fig. 9. The radiative heat transfer coefficient at $t = 300$ s for experiment #3.

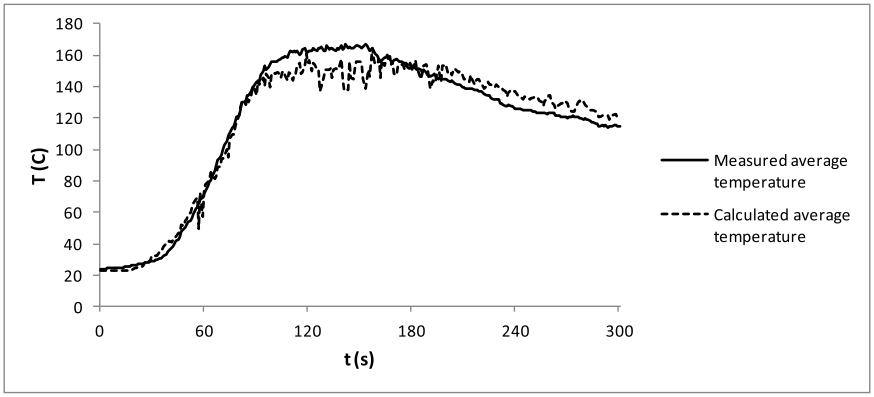

Fig. 10. The resulting average fire gas temperature of experiment #1. The measured average temperature was taken from the experiments of Hansen and Ingason (2010).

experiment #3. The large variations of the coefficient underlines the importance not to set the heat transfer coefficients constant, which is especially important in the case of multiple fires. Assuming a constant heat transfer coefficient and applying equation (1) is therefore questionable with respect to accuracy.

5.5. Fire gas temperature at the site of each individual fire

The fire gas temperature at the site of each individual fire will have a decisive impact on the resulting average fire gas temperature, as the temperature will serve as a starting point for the decaying trend following after the fire site. The fire gas temperature at the site of the fire will in turn depend on the heat release rate of the fire, the convective fraction of the heat release rate and the longitudinal ventilation velocity.

5.5.1. Heat release rate appearance of the individual fires

Based upon the measurements of reference experiment #4, the heat release rate of the first pile of wooden pallets could be adopted for the experiments involving multiple piles of pallets as well. But the question is what fire growth rate and maximum heat release rate should be assigned to the piles of wooden pallets further downstream?

Hansen (2017b) investigated the fire behaviour of the multiple fires in the model scale mine drift and found that the fire growth rate increased substantially for the fires found downstream of the initial fire. A number of fire growth rates were calculated for the second pile of wooden pallets based upon experimental data. The fire growth rate data from the paper by Hansen (2017b) were used in the ensuing calculations. The fire growth rate of piles with a free distance greater than 0.7 m, was assumed to be 0.035 kW/s^2.

An increasing irradiance at the ensuing piles of wooden pallets, will lead to an increasing maximum heat release rate of these piles. If assuming that the maximum heat release rate of the fourth pile of wooden pallets occurred at the same time as the overall maximum heat release rate occurred, the time to maximum heat release rate of the fourth pile can be calculated (as the ignition time of the fourth pile is known beforehand). Applying the fire growth rates from Hansen (2017b), the maximum heat release rate of the fourth pile can be calculated. Assuming a linear development of the maximum heat release rates of the four piles, the maximum heat release rates of the second and third pile can be calculated.

Applying all the above assumptions, the resulting average fire gas temperature came fairly close to the measured temperature and can be seen in the following part on multiple fires below. But the number of assumptions are considerable and so are the uncertainties connected with the assumptions.

When it comes to modelling the average fire gas temperature in a mine drift with multiple fires, one of the major challenges would be to obtain fire growth rate and maximum heat release rate data for the adjacent fuel items. Obtaining this data is of outmost importance as the appearance of the individual heat release rate curves will largely dictate the average fire gas temperature. Further studies into the fire growth rate and maximum heat release rates of multiple fires are highly recommended.

5.5.2. Convective fraction of heat release rate

The convective fraction of the heat release rate in equation (3) – i.e. $\frac{2}{3}$ – is based upon earlier conducted fire experiments in a copper mine (Ingason, Gustavsson, & Dahlberg, 1994) and will vary depending on what type of fuel that is involved in the fire. Initial calculations resulted

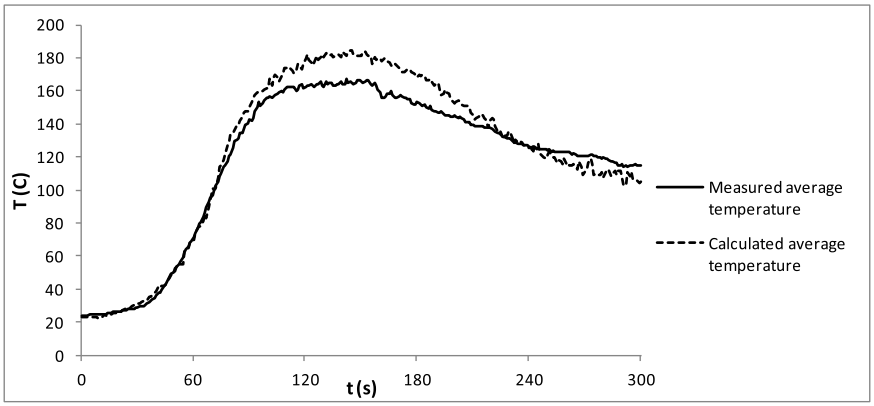

Fig. 11. The resulting average fire gas temperature of experiment #4. The measured average temperature was taken from the experiments of Hansen and Ingason (2010).

in average fire gas temperatures distinctly higher than the measured temperatures and therefore the convective fraction of the heat release rate was analysed further. Applying the following expression (Dahlberg, 1994):

$$\dot{Q}_{\text{conv}} = \dot{m}_{mix} \int_{T_a}^{T_g} c_{p,mix}(T)\mathrm{d}T \tag{24}$$

an average convective fraction of 0.5 was calculated applying data from the model scale experiments. The resulting average fire gas temperatures showed clear improvements in the accuracy. The selection of convective fraction of the heat release rate must be done with caution and to be preceded by an analysis.

5.6. Single fire source

The initial calculations comprised the three reference tests, where the longitudinal ventilation velocity was varied. The included parameters were analysed (see earlier parts of this paper), the findings implemented and the resulting average fire gas temperature curves were compared with the measured temperatures. The resulting temperature curves can be seen in Figs. 10–12. The calculated average temperatures of experiments #1 and #4 correlated very well with the measured temperatures during the growth phase, while the calculations of experiment #12 over predicted the temperatures during the growth phase.

During the period with maximum heat release rate (and corresponding average fire gas temperature), the calculations of experiments #1 and #12 under predicted the resulting average fire gas temperature, while the calculations of experiment #4 led to over predicted temperatures. The over prediction of the fire gas temperature in experiment #4 could be due to the increase in the radiative heat flux of the flame compared with experiments #1 and #12. This increase in the radiative heat flux from the flame is seen in Fig. 13, where experiment #4 (u = 0.6 m/s) displays a distinctly higher heat flux than experiment #1 (u = 0.3 m/s) and experiment #12 (u = 0.9 m/s) predominantly during the peak heat flux. The increase in the flame radiation will mostly have an effect of the immediate surroundings and not further downstream. The increase in the flame radiation will at the same time be at the expense of the convection and radiation of the fire gases, which in turn has more influence on the temperatures further downstream. When performing the calculations it became evident that the flame radiation to the surrounding construction did not influence the average fire gas temperature to any large extent, but given the variations of the flame radiation and its effect on the energy available for radiative and convective heat transfer from the fire gases the flame radiation will still have to be accounted for in the calculations.

During the decay phase, the calculations of experiment #1 led to over predicted average temperatures, the corresponding temperatures of experiment #12 was under predicted and the temperatures of experiment #4 was initially over predicted and later under predicted. The reason behind the varying results of the three cases is unclear and will have to be investigated further.

Despite the difference between the calculated temperatures and the measured temperatures, the differences are relatively small and the results are similar.

5.7. Multiple fire sources

The multiple fire scenario represents a highly variable scenario, as opposed to a single fire scenario where the average fire gas temperature

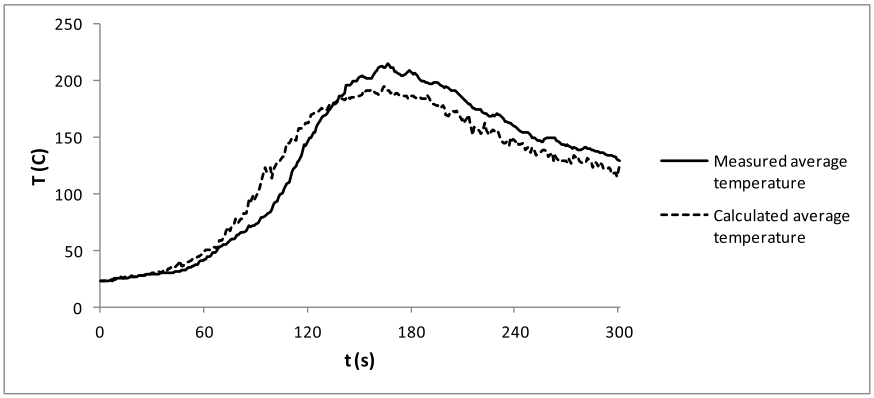

Fig. 12. The resulting average fire gas temperature of experiment #12. The measured average temperature was taken from the experiments of Hansen and Ingason (2010).

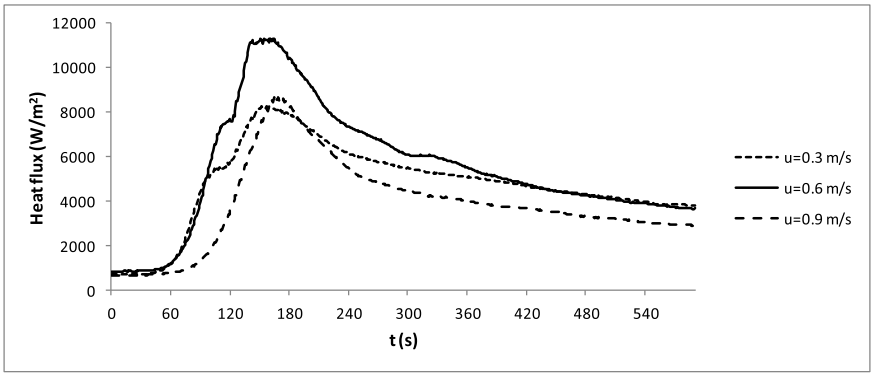

Fig. 13. The measured heat flux at floor level, 1 m downstream of the burning pile of pallets. The measured heat flux values were taken from the experiments of Hansen and Ingason (2010).

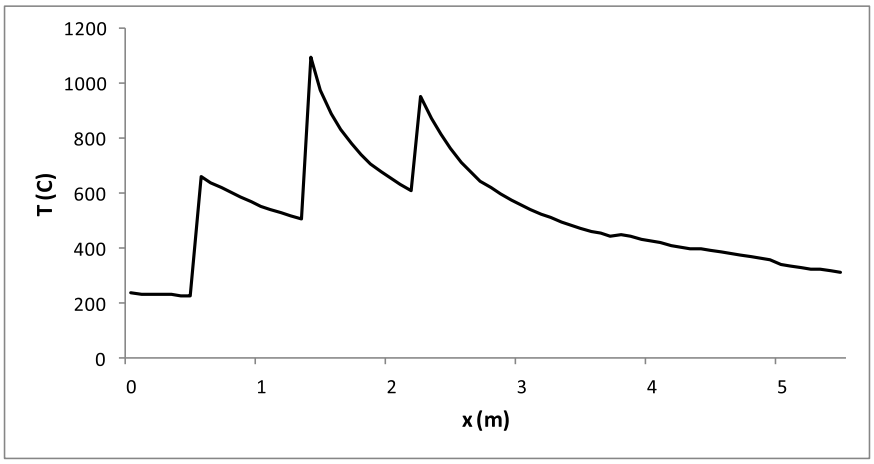

Fig. 14. The average fire gas temperature in experiment #3 at $t = 200$ s.

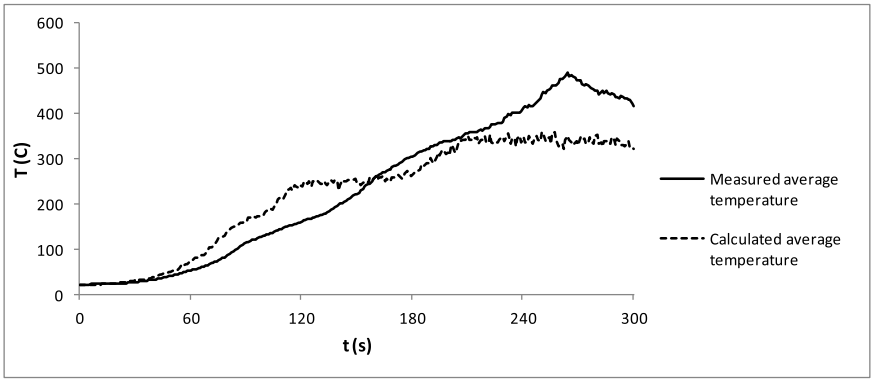

Fig. 15. The average fire gas temperature at pile B in experiment #3. The measured average temperature was taken from the experiments of Hansen and Ingason (2010).

will follow an exponentially decaying function starting from the site of the fire. Fig. 14 displays the variation of the average fire gas temperature along the model scale mine drift in experiment #3 at $t = 200$ s. Obviously, an expression of lumped characteristics will not be suitable for this type of scenario as the fires upstream will affect the fires downstream. The quasi-steady model used in this paper is clearly suitable for this type of scenario, with a number of highly varying parameters both spatially and temporally such as the heat transfer coefficients, ambient temperature and fire gas emissivity.

The resulting average fire gas temperatures during the initial 300 s at pile B for experiments #3 and #11 can be seen in Figs. 15 and 16. The resulting temperature graphs of experiment #3 and #11 are displayed as they represent the scenario with the shortest average distance between the piles of wooden pallets (experiment #3) and the longest average distance (experiment #11).

In both cases the calculated average fire gas temperature correlate fairly well with the measured temperature, except for the period when the fourth pile peaked in the heat release rate. During the peak period, the calculations led to under predicted fire gas temperatures. Besides the uncertainties connected with quantifying the heat release rate of the second, third and fourth pile of pallets (i.e. fire growth rate and maximum heat release rate) described earlier, some of the differences between the calculated and the measured temperature could be attributed to the use of the heat release rate of experiment #4 for the first pile of

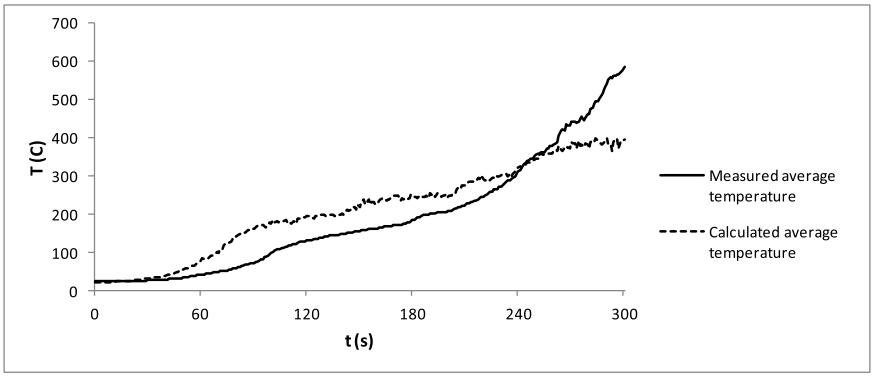

Fig. 16. The average fire gas temperature at pile B in experiment #11. The measured average temperature was taken from the experiments of Hansen and Ingason (2010).

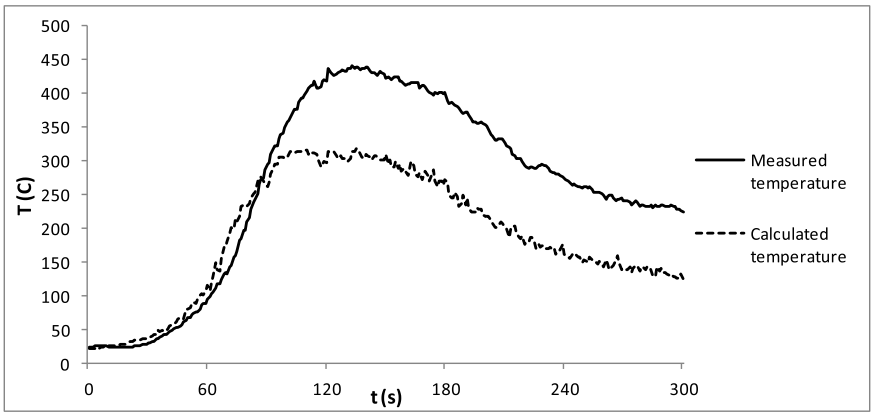

Fig. 17. The average fire gas temperature at pile A in experiment #4. The measured average temperature was taken from the experiments of Hansen and Ingason (2010).

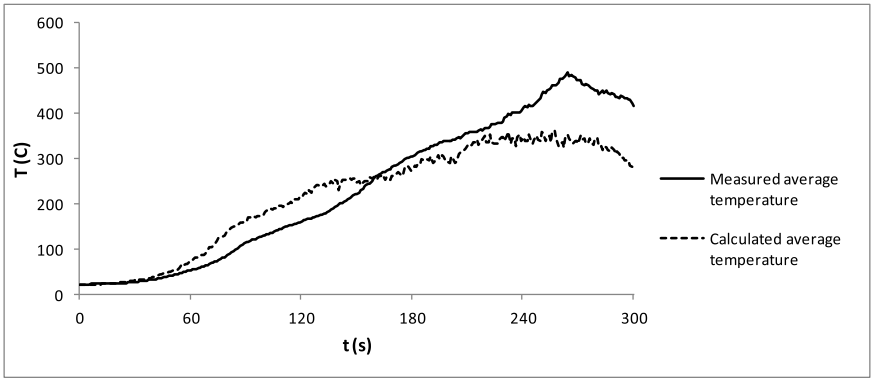

Fig. 18. The average fire gas temperature at pile B in experiment #3 with increased fire growth rate for the third and fourth pile of pallets. The measured average temperature was taken from the experiments of Hansen and Ingason (2010).

wooden pallets in the multi fire scenarios. The heat release rate in experiment #4 is connected with the longitudinal ventilation velocity of that specific experiment. Even though the longitudinal ventilation velocity in experiment #4 did not deviate particularly from the multi fire experiments, there are differences in magnitude which would affect the corresponding heat release rate and thus also the average fire gas temperature.

The distinct differences between the calculated and measured temperatures during the peak period, as well encompassing the peak heat release rate period of the fourth pile of pallets it also includes the period when the distance between the last pile of pallets to pile B is the shortest. When comparing the calculated average fire gas temperature of experiment #4 at pile A (see Fig. 2) with the measured temperatures, it was found that the calculations clearly under predict the average temperature (see Fig. 17 for the average fire gas temperature at pile A). A possible explanation of the under predicted temperatures at pile B could be that the fire growth rate of the third and fourth pile was higher than earlier assumed. It can be assumed that a fire growth rate of 0.09 kW/s^2 for the third pile and 0.1 kW/s^2 for the fourth pile resulted in the average fire gas temperature – for experiment #3 – found in Fig. 18. As can be seen the increase in fire growth did increase the resemblance between the calculated temperature and the measured temperature, but the distinct difference during the peak period still remained. If applying a flame tip temperature criterion of 500 K above ambient (Heskestad, 2008) and studying the flame length during the peak period, it was found that during the peak period three out of five

thermocouples were either engulfed by flames or that flame impingement occurred. It is therefore clear that the difference in temperature during the peak period was largely due to flame impingement, which also applies for the temperature difference at pile A. As the distance increases, the risk of flame impingement will decrease as will the under prediction of the temperature. The equivalent full-scale distance between the last pile of pallets and pile B is 45.75 m in the case of experiment #3 and 30.75 m in the case of experiment #11.

The multiple fire scenario is distinguished by an exponentially decaying average fire gas temperature and also by the sudden increase at the site of each individual fire. The ambient temperature of the fires further downstream will be equal to the average fire gas temperature of the fires further upstream. This will lead to a continued increase of the fire gas temperature for every individual fire downstream and an overall escalating average fire gas temperature.

6. Conclusions

Analysis of the average fire gas temperature for multiple fire scenarios in a mine drift with longitudinal ventilation was conducted. The analysis was based upon earlier conducted model scale fire experiments in a scaled down mine drift. A quasi-steady model was applied as a number of parameters were transient, such as the heat release rate and the longitudinal ventilation velocity.

It is found that the calculated average fire gas temperature of the quasi-steady model correlate fairly well with the measured temperature, except for the period when the pile of pallets closest to the measuring point peaked in heat release rate. During this period the average fire gas temperatures were under predicted. The under prediction is likely due to flame impingement as the distance to the nearest fire decreases. One uncertainty of the calculations is the fire gas temperature at the site of each individual fire, which will have a decisive impact on the resulting average fire gas temperature (serving as a starting point for the decaying temperature trend after the fire site). The fire gas temperature at the site of the fire will largely depend on the heat release rate of the fire and this is where the uncertainties are found. The challenge would be to obtain fire growth rate and maximum heat release rate data for the adjacent fuel items in order to depict the heat release rate as accurately as possible. The highly variable scenario with multiple fires, increasing fire growth rates and maximum heat release rate for each individual fire further complicates the situation. Further studies into the fire growth rate and maximum heat release rates of multiple fires are recommended.

In addition to the appearance of the heat release rate, the convective fraction of the heat release rate was found to have a significant influence on the resulting average fire gas temperature. The convective fraction of the heat release rate must be chosen with caution and must be preceded by thorough analysis. The fire gas emissivity cannot be assumed at a constant value as it was found to have a large and undesired impact on the average fire gas temperature during periods with higher temperatures. The variations of the fire gas emissivity due to temperature changes must be accounted for.

The multiple fire scenario is distinguished by it being a highly transient fire scenario, with an exponentially decaying average fire gas temperature and also by the sudden increase at the site of each individual fire. The longitudinal ventilation which in the case of a single fire scenario will have a cooling effect on the fire gases when mixing with the gases, will have much less of a cooling effect as the temperature of the longitudinal flow becomes equal to the average fire gas temperature of the fires upstream. The ambient temperature of the fires further downstream will thus be equal to the average fire gas temperature of the fires further upstream. This will lead to a continued increase of the fire gas temperature for every individual fire downstream and an overall escalating average fire gas temperature.

A fire in an underground mine will always pose a risk. However, through knowing the average fire gas temperature at certain distances from a set of multiple fires, the smoke spread and smoke behaviour in an area could be analysed and appropriate measures could be taken with respect to the egress safety and the smoke control. This will increase the safety of the miners as well as the fire personnel.

Ethical statement

Authors state that the research was conducted according to ethical standards.

Funding

None.

Conflict of interest

None declared.

Appendix A. Supplementary data

Supplementary data related to this article can be found at https://doi.org/10.1016/j.jsm.2018.08.001.

References

Beard, A., & Carvel, R. (2005). *The handbook of tunnel fire safety*. London: Thomas Telford Ltd.

Bhatti, M. S., & Shah, R. K. (1987). Turbulent and transition flow convective heat transfer in ducts. In S. Kakaç, R. K. Shah, & W. Aung (Eds.). *Handbook of single-phase convective heat transfer*. Wiley-Interscience.

Chang, X., & Greuer, R. E. (1985). Simplified method to calculate the heat transfer between mine air and mine rock. *Proceedings of the 2nd US Mine Ventilation Symposium* (pp. 429–438). Reno: CRC Press.

Chang, X., & Greuer, R. (1987). A mathematical model for mine fires. *Proceedings of the 3rd Mine Ventilation Symposium* (pp. 453–462). University Park: Society for Mining Metallurgy.

Dahlberg, M. (1994). *Error analysis for heat release measurements with the SP industry calorimeter. SP Report 1994:29*Borås: Swedish National Testing and Research Institute.

Dziurzynski, W., Tracz, J., & Trutwin, W. (1988). Simulation of mine fires. In A. D. S. Gillies (Ed.). *4th International Mine Ventilation Congress, Brisbane Australia 3–6 July 1988* (pp. 357–363). Melbourne: Australasian Institute of Mining and Metallurgy.

Hansen, R. (2017a). *Heat losses of fire gases in a mine drift with rough rock surface and forced longitudinal ventilation.* Brisbane: The University of Queensland.

Hansen, R. (2017b). *Multiple fires in a mine drift with longitudinal ventilation.* Brisbane: The University of Queensland.

Hansen, R., & Ingason, H. (2010). *Model scale fire experiments in a model tunnel with wooden pallets at varying distances. Research Studies in Sustainable Technology 2010, Vol. 8.* Västerås: Mälardalen University.

Hansen, R., & Ingason, H. (2011). An engineering tool to calculate heat release rates of multiple objects in underground structures. *Fire Safety Journal, 46*(4), 194–203. https://doi.org/10.1016/j.firesaf.2011.02.001.

Hansen, R., & Ingason, H. (2012). Heat release rates of multiple objects at varying distances. *Fire Safety Journal, 52*, 1–10. https://doi.org/10.1016/j.firesaf.2012.03.007.

Heskestad, G. (2008). Fire plumes, flame height and air entrainment. In P. J. Dinenno, D. Drysdale, C. L. Beyler, W. D. Walton, & R. L. P. Custer (Eds.). *The SFPE Handbook of Fire Protection Engineering*(4th ed.). Quincy, Mass: National Fire Protection Association 2-1–2.20.

Hottel, H. C. (1954). Radiant heat transmission. In W. H. McAdams (Ed.). *Heat transmission (chapter 4)*. New York: McGraw-Hill.

Incropera, F. P., Dewitt, D. P., Bergman, T. L., & Lavine, A. S. (2007). *Fundamentals of heat and mass transfer* (6th ed.). Hoboken: John Wiley & Sons Inc.

Ingason, H. (2005). *Model scale tunnel fire tests. SP report 2005:49*Borås: Swedish National Testing and Research Institute.

Ingason, H., Gustavsson, S., & Dahlberg, M. (1994). *Heat release rate measurements in tunnel fires. SP Report 1994:08*Borås: Swedish National Testing and Research Institute.

Ji, J., Wan, H., Gao, Z., Fu, Y., Sun, J., Zhang, Y., et al. (2016). Experimental study on flame merging behaviors from two pool fires along the longitudinal centerline of model tunnel with natural ventilation. *Combustion and Flame, 173*, 307–318. https://doi.org/10.1016/j.combustflame.2016.08.020.

McPherson, M. J. (1986). The analysis and simulation of heat flow into underground airways. *International Journal of Mining and Geological Engineering, 4*(3), 165–196. https://doi.org/10.1007/BF01560715.

Mills, A. F. (1962). Experimental investigation of turbulent heat transfer in the entrance

region of a circular conduit. *Journal of Mechanical Engineering Science, 4*(1), 63–77. https://doi.org/10.1243/JMES_JOUR_1962_004_010_02.

Newman, J. S., & Tewarson, A. (1983). Flame propagation in ducts. *Combustion and Flame, 51*, 347–355. https://doi.org/10.1016/0010-2180(83)90112-8.

Simode, E. (1985). Simulation of thermal and aerodynamic effects of a fire in a complex underground ventilation network. *Proceedings of the 2nd US Mine Ventilation Symposium* (pp. 455–459). Reno: CRC Press.

Wan, H., Gao, Z., Ji, J., Li, K., Sun, J., & Zhang, Y. (2017). Experimental study on ceiling gas temperature and flame performances of two buoyancy-controlled propane burners located in a tunnel. *Applied Energy, 185*(1), 573–581. https://doi.org/10.1016/j.apenergy.2016.10.131.

Wolski, J. K. (1995). Modeling of heat exchange between flowing air and tunnel walls. In A. M. Wala (Ed.). *Proceedings of the 7th US Mine Ventilation Symposium, June 5–7, 1995, Lexington, Kentucky* (pp. 207–212). Littleton, CO: Society for Mining, Metallurgy, and Exploration.